Lecture 4:
Case study: Black Hole Mass Estimates from CASTLES lenses

Emilio E. Falco
Smithsonian Astrophysical Observatory
F. L. Whipple Observatory
670 Mt. Hopkins Rd.
Amado, AZ 85645, USA

Inspiration:
"Black Hole Mass Estimates Based on C IV are Consistent with Those Based on the Balmer Lines"
R.J. Assef et al. 2012, ApJ 742, 93 (A12)

1. GOALS

1. Measure black hole (BH) masses using quasar spectra.

2. Start with the Greene, Peng & Ludwig (2010; GPL10) sample, add near-IR spectroscopic data, consistently analyzed high SNR optical spectra, and consistent continuum luminosity estimates at 5100Å.

3. Demonstrate that BH mass estimates based on the FWHM of C IV show a systematic offset with respect to estimates from the line dispersion σ_l of the same emission line, but not with those obtained from the FWHM of Balmer lines Hα and Hβ.

4. Test the reliability of C IV mass estimates by systematic comparison with Balmer line estimates for the same sources.

5. Because at higher redshifts the better-calibrated Hα and Hβ lines are in the near-IR, obtain IR spectra of distant, lensed quasars. Measure FWHMs of Hα and Hβ to estimate the mass of the BH in each case.

2. GALAXIES AND BLACK HOLES

Massive galaxies have supermassive BHs at their centers. The mass of the central BH correlates well with the luminosity of the spheroidal component of the host (Marconi & Hunt 2003; Graham 2007) and with its velocity dispersion (Ferrarese & Merritt 2000; Gebhardt et al. 2000; Tremaine et al. 2002; Gültekin et al. 2009; Graham et al. 2011). Both properties involve scales a few orders of magnitude larger than the sphere of influence of the BH, but they are linked. Theory accounts for the correlation through co-evolution of the galaxy and its BH: accretion induced by galaxy mergers regulates the BH's growth, but feedback regulates the growth of the galaxy by quenching star formation and removing cold gas (e.g., Shankar et al. 2009), a process at work early in the universe, at $z \sim 6$ (e.g., Maiolino et al. 2012).

Direct measurements of BH masses in inactive galaxies are possible only for a small number of nearby objects because it is necessary (e.g., Merritt & Ferrarese 2001; Gültekin et al. 2009) to resolve the BH's sphere of influence to determine its mass from the kinematics of stars and gas nearest it. AGNs offer a different estimator of BH masses at any distance. Type 1 AGNs (face-on disk) show bright broad emission lines from gas in the broad line region (BLR), near the central BH but outside the hot accretion disk. The large line-widths are caused by Doppler broadening from the orbital velocity of the gas around the BH. Measuring the mass of the BH from the width of the broad lines is possible if the distance $D_{\rm BH-BLR}$ from the BLR to the BH is known.

$D_{\rm BH-BLR}$ can be estimated with reverberation mapping (RM) (Blandford & McKee 1982; Peterson 1993). We discussed RM in Lecture 3.

The timescale for significant variability in AGNs increases with BH mass (e.g., Vanden Berk et al. 2004; Wilhite et al. 2008; Kelly et al. 2009; MacLeod et al. 2010), making it much more time intensive to apply RM to the luminous quasars with the most massive BHs. For example, MacLeod et al. (2010) find that for quasars with $M_{\rm BH} = 10^8\ M_\odot$ to $10^9\ M_\odot$ ($M_i \approx -23$ to -25.5 mag), the rest-frame timescale Δt required for an RMS variability amplitude of 0.1 mag is $\sim 45 - 125$ days. Time dilation at higher redshifts further complicates the matter. However, $D_{\rm BH-BLR}$ correlates well with the continuum luminosity of the AGN (see, e.g., Kaspi et al. 2000, 2005; Bentz et al. 2006, 2009; Zu et al. 2010). Therefore, BH masses can be estimated for distant broad-line quasars for which RM is infeasible. Masses estimated in this way are referred to as single epoch (SE) BH mass estimates.

It is easier to obtain optical rather than UV or IR spectra, so SE BH masses are typically estimated from Hβ and Hα lines and the continuum luminosity at 5100Å at $z \lesssim 0.7$. The overlap with RM targets yields a very accurate calibration of these SE mass estimators. At $z > 0.7$, the lines are shifted to the IR, and most mass estimates are then based on the UV Mg II λ2798 and C IV λ1549 broad emission lines and the continuum luminosities at 3000Å for Mg II and 1450Å or 1350Å for C IV. Unlike the Balmer lines, the UV lines lack large local calibration samples because of the difficulty of obtaining UV-based RM measurements. VP06 calibrated a C IV-based mass estimator based on local RM AGNs with space-based UV spectra. However, there are still concerns about whether the C IV velocity widths are solely due to gravity or if there are bulk flows due to winds of ejected material. The impact of these effects on the accuracy of C IV-based BH mass estimates is unknown.

GPL10 presented near-IR spectroscopy for a sample of lensed quasars from CASTLES whose C IV or Mg II BH masses had been estimated in Peng et al. (2006). GPL10 measured the FWHM of Hβ and Hα for these objects and found no biases between BH masses estimated from these lines and those estimated from C IV. Their sample covered a small range in BH mass, so they could not measure a mass dependent slope in the relation between the masses. To improve on this, the approach of A12 was:

- Add Balmer-line based BH mass estimates for the lens SDSS1138+0314 and make revised estimates based on new, higher SNR, spectra of HS0810+2554 and SBS0909+532. A12 obtained near-IR observations for SDSS1138+0314 and HS0810+2554 with LBT/LUCIFER (LUCIFER; Seifert et al. 2003; Ageorges et al. 2010) and for SBS0909+532 they used the UV through IR observations of Mediavilla et al. (2010).
- Make consistent C IV BH mass estimates from high SNR spectra using the original observations in Peng et al. (2006), other published or unpublished spectra, or new spectra for the sample.
- Obtain continuum luminosities at 5100Å for all objects in the sample in a consistent manner. This allows A12 to include the lenses SDSS0246–0825, HS0810+2554 and Q2237+030, excluded by GPL10. Thus, they expanded this sample with both C IV and Balmer lines mass estimates from 7 to 12 quasars and the mass range covered by ~ 0.5 dex.

3. SAMPLE

A12 selected 12 lensed quasars from CASTLES with high quality UV/optical, typically ground-based, spectra of C IV and either published near-IR spectra of the Balmer lines or IR magnitudes bright enough to obtain such spectra. They used the sample of GPL10, who observed most of these lenses in the near-IR with the Triplespec spectrograph at APO. The wavelength range of the spectra is $0.95 - 2.46\,\mu$m with $R = 35$. Hα and Hβ were observable in one of the atmospheric windows. Although GPL10 considered objects with a large span of redshift and reddening, they limit the sample to objects with sufficiently high redshift and small enough reddening for C IV emission to be observable in ground-based UV/optical spectra. GPL10 presented FWHM velocity width measurements for all but 3 of the objects in their sample. For these latter objects, SDSS0246–0825, HS0810+2554 and Q2237+030, A12 measured the continuum luminosity and estimated BH masses so they were included in their sample.

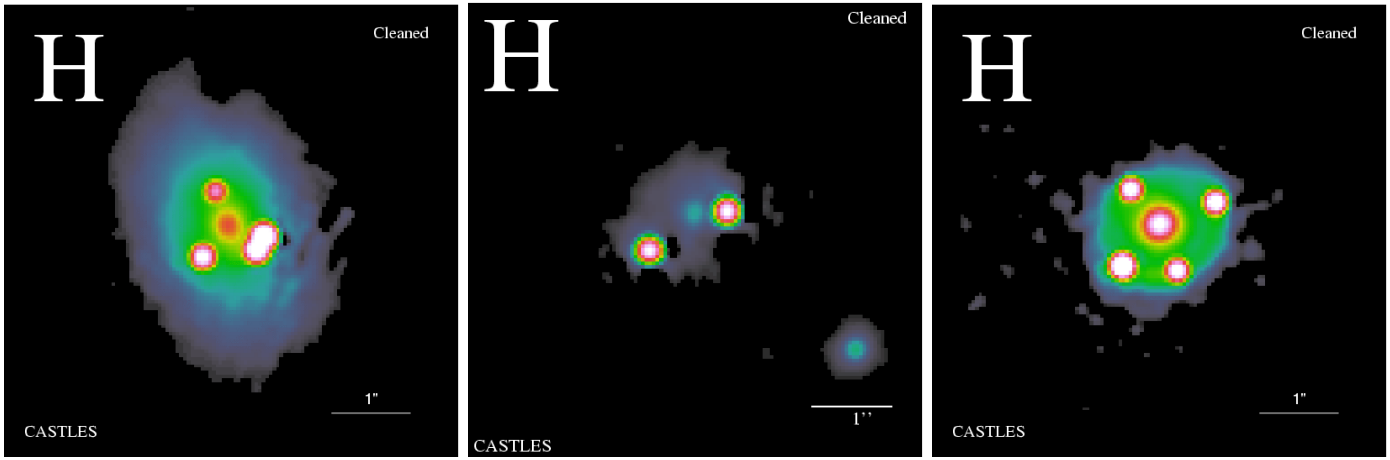

Fig. 1.— A sub-sample of A12 targets for measuring BH masses. 0 CASTLES H-band images of HS0810, SBS0909 and SDSS1138.

Table 1. Lens Magnifications and Continuum Luminosities, Literature UV/optical spectra.

Object	Ref.	z	Image Magnification				m_H (unmag.)	$\log \lambda L_\lambda$ / erg s^{-1}		
			A	B	C	D	(mag)	1350Å	1450Å	5100Å
Q0142–100	*a*	2.72	3.3	0.4	···	···	16.56	46.83	46.76	46.27
SDSS0246–0825	*a*	1.69	26.9	8.9	···	···	20.39	···	44.53	44.59
HS0810+2554	···	1.51	47.2	51.1	13.5	7.7	18.72	···	44.44	44.84
SBS0909+532	*b*	1.38	1.7	1.5	···	···	15.18	46.08	46.05	46.31
Q0957+561	*c*	1.41	3.1	1.7	···	···	16.51	46.31	46.25	45.79
HE1104–1805	*d*	2.32	16.2	2.3	···	···	18.52	46.15	46.09	45.38
PG1115+080	*a*	1.72	19.6	18.7	3.2	4.9	19.13	···	45.47	44.93
SDSS1138+0314	*e*	2.44	7.3	3.7	5.2	6.9	20.65	44.83	44.77	44.81
H1413+117	*a*	2.55	8.2	6.8	6.8	3.4	18.05	45.73	45.78	45.63
B1422+231	*f*	3.62	6.6	8.2	4.3	0.3	16.55	46.83	46.74	46.42
FBQ1633+3134	···	1.52	2.7	0.7	···	···	16.85	45.65	45.64	45.72
Q2237+030	*g*	1.69	4.9	4.3	2.2	4.1	16.83	···	45.53	45.98

3.1. LUCIFER OBSERVATIONS

LUCIFER is a near-IR spectrograph and imager at the LBT with an overall wavelength range of $0.85 - 2.5\,\mu$m. A12 observed SDSS1138+0314 with it for a total integration time of 840s over 7 dithered exposures. The effective wavelength range was $1.49 - 2.4\,\mu$m. The slit was placed on images A and C of the lensed quasar, as well as part of the lens galaxy. The lens galaxy was not detected. The B9V star HIP 33350 was observed with the same configuration, to correct the quasar spectra for telluric absorption features. The seeing was $\sim 0\farcs8$.

A12 also obtained near-IR spectra in the H and K bands and in the J-band for HS0810+2554 (Fig. 3) with LUCIFER. Finally, they added the J- and H-band observations of SBS0909+532 in Mediavilla et al. (2010) (Fig. 4).

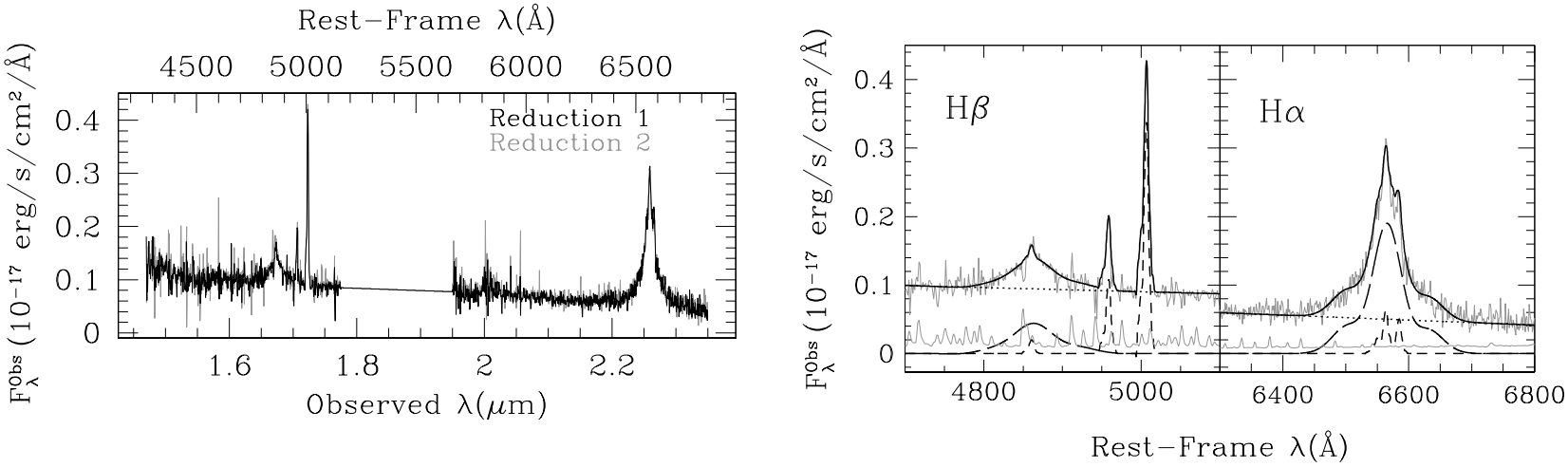

Fig. 2.— Left: LUCIFER spectra of SDSS1138+0314. Right: Left panel, Hβ region. Overlaid are the best-fit continuum (*black dotted line*) and narrow (*black short-dashed line*) and broad line components (*black long-dashed line*) and their sum (*black solid line*) and the error spectrum (*thin gray solid line*). Note the [O III] $\lambda\lambda$4959, 5007 emission near 5000Å. Right panel, as the Left panel but for Hα.

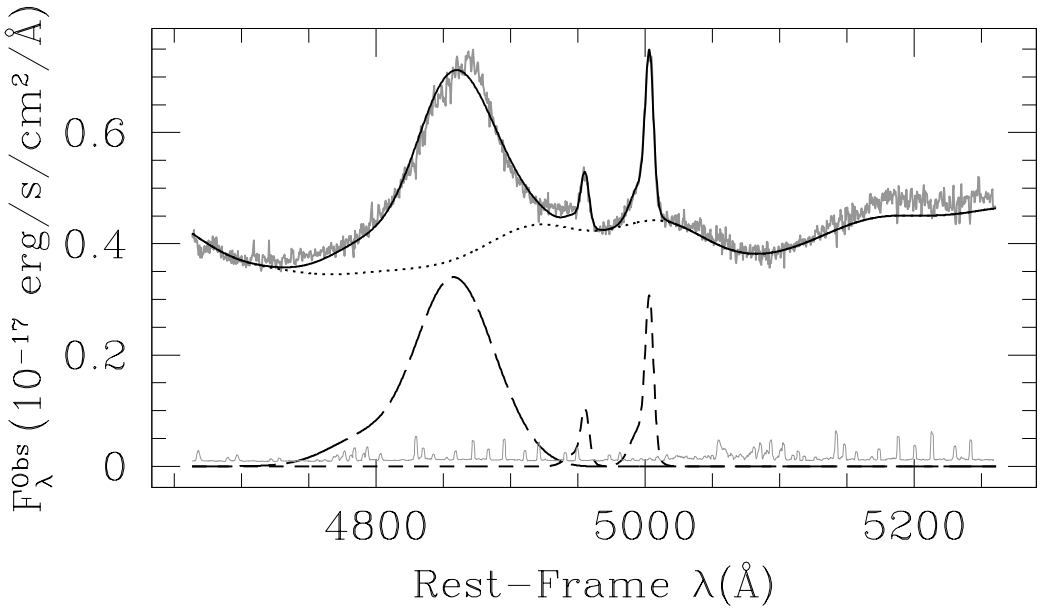

Fig. 3.— LUCIFER *J*-band spectrum of HS0810+2554 (*gray solid line*). Overlaid are the best-fit continuum and FeII emission (*black dotted line*), narrow line emission (*black short-dashed line*), broad line component (*black long-dashed line*) and their sum (*black solid line*) and the error spectrum (*thin gray solid line*).

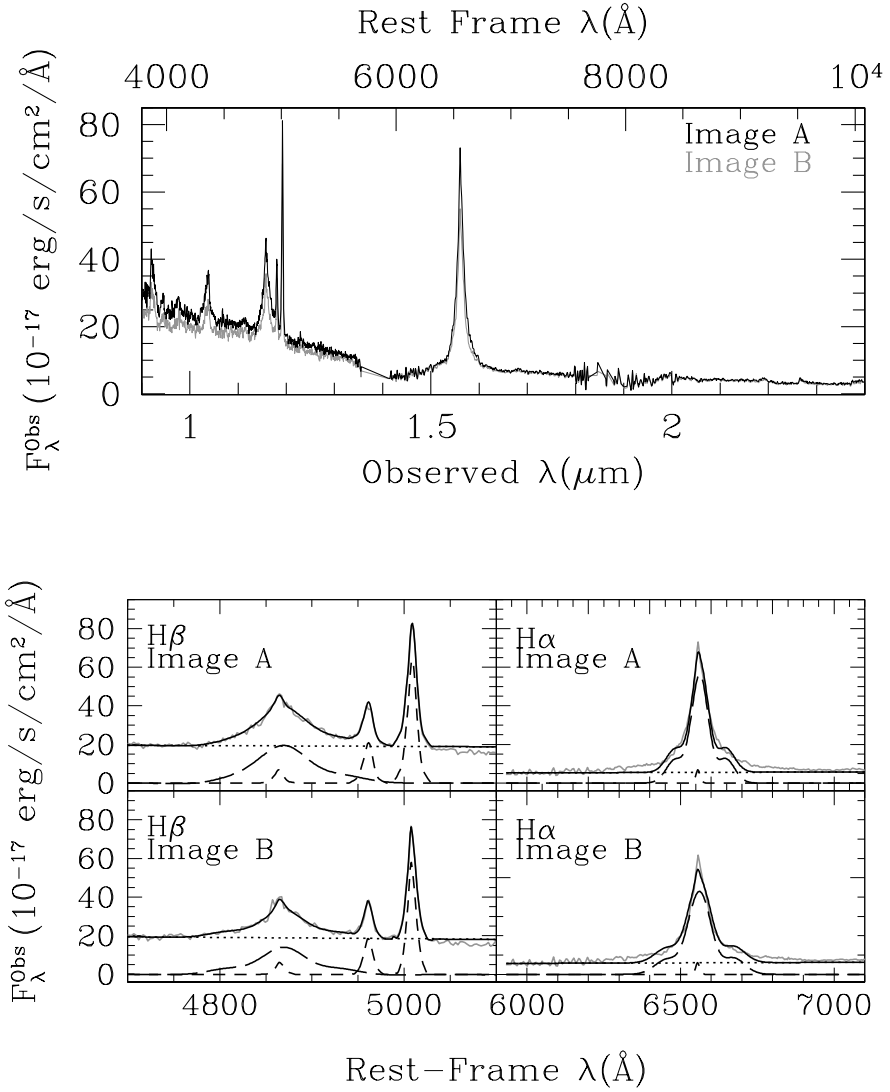

Fig. 4.— LIRIS near-IR spectra of images A and B of SBS0909+532 of Mediavilla et al. (2010). Top: full spectra. Bottom: Hα and Hβ spectral regions for A and B. Overlaid are the best-fit continuum and narrow- and broad-line components, as well as their sum.

3.2. UV/OPTICAL SPECTRA

For most of the GPL10 sample and for SDSS1138+0314, there were high SNR optical spectroscopic observations in the literature (see Table 3, except for HS0810+2554. A12 obtained optical spectra with the MDM 2.4m Hiltner telescope and the Boller & Chivens CCD Spectrograph (CCDS). The spectra of our sub-sample of A12 targets are in Fig. 5.

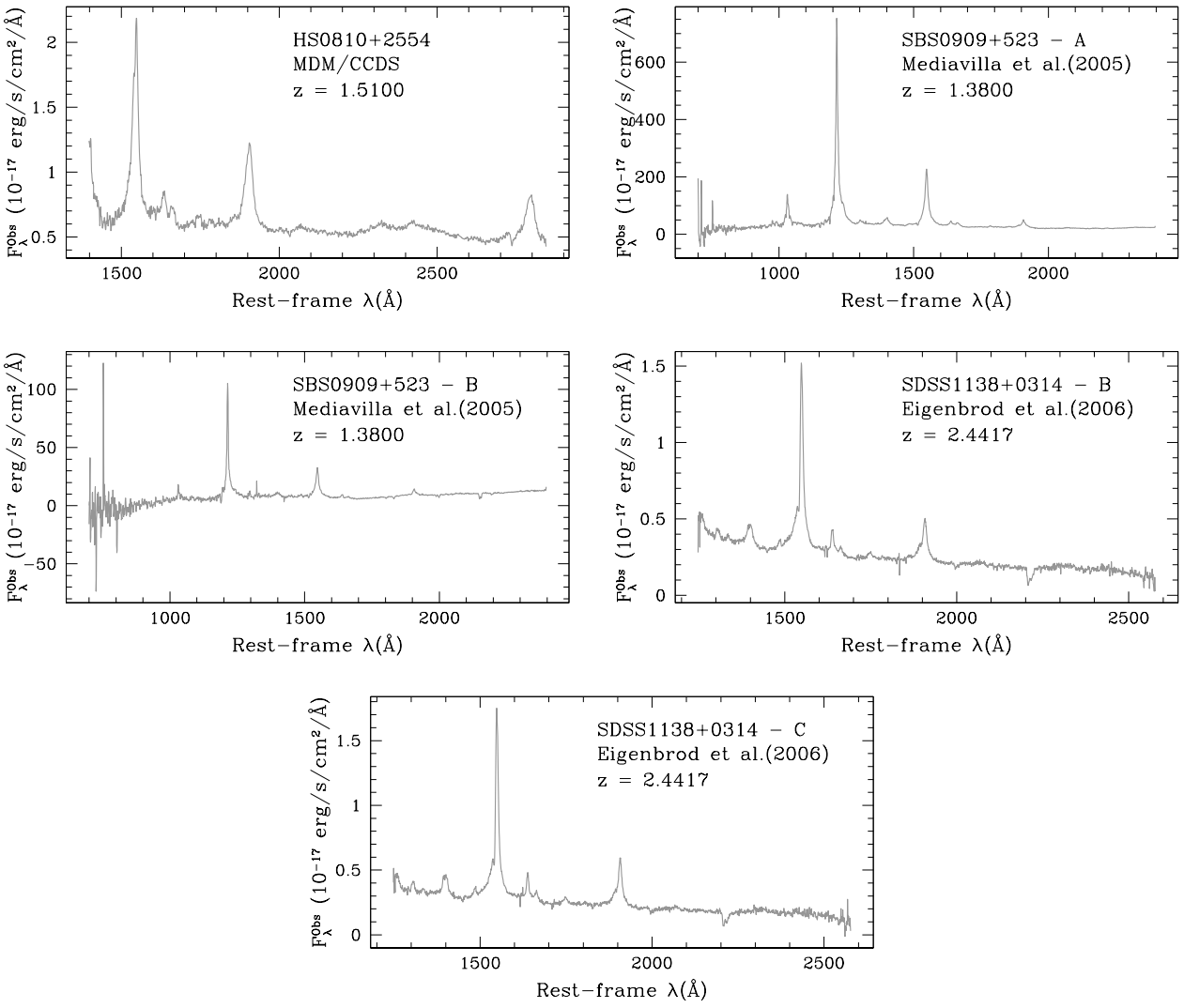

Fig. 5.— UV/optical spectra of our sub-sample objects in A12. Each panel shows the full spectrum, the object's name and its redshift.

4. MODELS AND MEASUREMENTS

4.1. LINE-WIDTHS

A12 tested two prescriptions, **A** and **B** for removing the continuum and blended emission from C IV emission line profiles. **A** is as in VP06, where the shelf feature redward of C IV is considered part of the C IV line profile, but only the region within $\pm 10,000$ km s^{-1} of the peak is considered. The continuum is fit by linearly interpolating between the two continuum windows in the ranges 1425−1470 and 1680−1705Å. In **A**, He II and O III] emission is not explicitly removed, but this is unimportant because of the limited velocity range. **B** is as prescription (3) of Fine et al. (2010); they fit the λ1600 feature as part of the continuum. However, the red continuum region matches the minimum between C IV and the λ1600 feature. **A** yields broader estimates of the C IV line-width than **B**.

For spectra with mild absorption features, bad pixels, and/or significant night sky line residuals, A12 used a polynomial up to 3rd order to interpolate across before measuring the line widths. They did not attempt to remove narrow-line emission from C IV λ1549, because it is very weak and cannot be reliably isolated (Wills et al. 1993), and the separate lines of the C IV doublet are unresolved in AGN spectra (see VP06). They characterized the line width by both its FWHM and line dispersion (σ_l, the second moment of the line profile). The widths were measured directly from the actual or interpolated spectrum following Peterson et al. (2004).

A12 also fit the original or interpolated line profiles with a 6th-degree Gauss-Hermite (GH) polynomial. These fits to emission-line profiles mitigate low SNR. FWHM and σ_l measurements of the C IV λ1549 line are in Table 2 for both prescriptions. A12 used the line widths measured directly from the data for the subsequent BH mass calculations. C IV λ1549 widths were smaller than those in GPL10 for objects where both groups used SDSS spectra. The likely origin of the discrepancy is that GPL10 fit a narrow line component as part of the C IV profile, which yields larger FWHM values for the broad component.

Line widths of Hβ and Hα are in Table 2. A12 measured them from the near-IR spectra with the C IV procedure except that (1) the best GH polynomial fit was used for all line-width measurements, save for Hα for SBS0909+532, because the SNR of the near-IR data was too low to measure directly from the data; (2) blended emission-line components were removed from each spectrum before the line width was measured; and (3) a power-law continuum was fitted to the Hβ spectrum of HS0810+2554 because it was fitted simultaneously with additional blended emission-line components over a larger wavelength range.

Table 2. Velocity Widths

Object	Broad Emission Line Velocity Widths / 10^3 km s^{-1}							
	FWHM$_{\rm C\,IV}$–p.A	FWHM$_{\rm C\,IV}$–p.B	$\sigma_{l,\rm C\,IV}$–p.A	$\sigma_{l,\rm C\,IV}$–p.B	FWHM$_{\rm H\beta}$[†]	$\sigma_{l,\rm H\beta}$	FWHM$_{\rm H\alpha}$[†]	$\sigma_{l,\rm H\alpha}$
Q0142–100	5.20 ± 0.18	4.75 ± 0.22	3.67 ± 0.04	3.67 ± 0.07	2.70 ± 0.60*	···	3.80 ± 0.30*	···
SDSS0246–0825	4.43 ± 0.24	4.40 ± 0.22	3.09 ± 0.06	2.51 ± 0.04	2.50 ± 0.60	···	2.50 ± 0.20	···
HS0810+2554	3.68 ± 0.14	3.53 ± 0.16	3.40 ± 0.05	2.85 ± 0.08	4.40 ± 0.06	2.21 ± 0.04	3.80 ± 0.00	···
SBS0909+532	2.38 ± 0.08	2.36 ± 0.08	2.90 ± 0.04	2.82 ± 0.05	3.95 ± 0.17	2.20 ± 0.05	3.06 ± 0.34	5.24 ± 0.04
Q0957+561	3.68 ± 0.25	3.47 ± 0.08	3.27 ± 0.09	2.272 ± 0.007	3.30 ± 0.90	···	3.00 ± 0.20	···
HE1104–1805	6.08 ± 0.35	5.75 ± 0.05	3.84 ± 0.10	2.897 ± 0.004	3.80 ± 0.90	···	4.70 ± 0.20*	···
PG1115+080	4.98 ± 0.18	4.67 ± 0.13	3.68 ± 0.04	3.40 ± 0.04	4.40 ± 0.20	···	4.00 ± 0.10	···
SDSS1138+0314	>2.02 ± 0.15	>1.99 ± 0.18	>3.12 ± 0.04	>2.40 ± 0.11	3.93 ± 0.30	2.08 ± 0.18	2.57 ± 0.04	1.90 ± 0.05
H1413+117	>2.62 ± 0.95	>2.54 ± 0.37	>3.78 ± 0.15	>1.82 ± 0.07	6.70 ± 1.90	···	5.30 ± 0.80	···
B1422+231	5.81 ± 0.16	5.56 ± 0.02	3.70 ± 0.03	3.321 ± 0.006	6.10 ± 2.20*	···	···	···
FBQ1633+3134	>4.71 ± 0.18	>4.40 ± 0.16	>3.83 ± 0.06	>2.20 ± 0.06	4.60 ± 0.90*	···	4.10 ± 0.70	···
Q2237+030	3.96 ± 0.18	3.78 ± 0.12	3.49 ± 0.07	2.51 ± 0.05	3.80 ± 1.40	···	4.80 ± 0.60*	···

[†]Hα and Hβ line width measurements from Table 1 of GPL10, except for SDSS1138+0314, SBS0909+523 and HS0810+2554.

For objects without near-IR spectroscopic observations, A12 used the Hα and Hβ line widths of GPL10. Most of their FWHM estimates are reliable (Group I), except for a few (Group II) because (1) they were measured from very low SNR spectra, (2) the lines were not fully contained in the wavelength range of the spectra, and/or (3) A12 disagreed with the narrow-line component models subtracted before the line width was measured. Individual objects can be in both groups because these issues may affect only one of the Balmer lines. Also included in Group I are Hα and Hβ line-width measurements from the new IR spectra.

4.2. UNCERTAINTIES

The sources of uncertainties in line-width measurements are difficult to model, as they depend on the overall SNR, on the line profile and the presence of sky lines. A12 used Monte Carlo simulations to model uncertainties. Using the flux error per pixel in each spectrum and the best-fit GH line profile (except for the optical SDSS1138+0314 and SBS0909+532 spectra, A12 generated 1000 resampled spectra by adding random Gaussian deviates based on the error spectrum to the flux in each pixel of the GH model spectrum and then re-measured the line width. For the UV/optical spectra from the literature without an error spectrum, they estimated one by propagating the SNR of a small continuum window near the C IV λ1549 emission line to the overall spectrum.

The flux error δF_λ in a pixel at λ with flux F_λ is:

$$\delta F_\lambda \;=\; \sqrt{\frac{\lambda_c}{\lambda}\; F_{\lambda_c} F_\lambda}\; \mathrm{SNR}_c^{-1}, \tag{1}$$

where λ_c and F_{λ_c} are the average wavelength and flux per unit λ of the continuum window chosen, and SNR_c is the SNR per pixel in the chosen continuum window. The only source of error is taken to be Poisson fluctuations; the number of detected photons is $\propto F_\lambda (hc/\lambda)^{-1}$, with a constant empirically determined in the continuum window from SNR_c, λ_c and F_{λ_c}. This estimate neglects the sky background and strong absorption or emission sky lines. It also neglects changes in the instrument sensitivity as a function of λ and assumes a constant pixel λ-width, reasonable because the continuum SNR is measured next to each emission line.

4.3. LUMINOSITIES

A12 estimated continuum luminosities at 5100Å by fitting the AGN SED template of Assef et al. (2010) to the unmagnified quasar magnitudes obtained from CASTLES NICMOS imaging, corrected for the lens magnification. They modeled each system using the astrometry and lens galaxy photometry from the CASTLES *HST* WFPC2 and NICMOS observations, see Lehár et al. (2000). Table 3 lists the magnifications used for each object in the sample.

A12 only removed Galactic foreground extinction, as the requirement that C IV be observable in the UV/optical eliminates the presence of dust absorption. For all 4-image lenses, they estimated the source flux for all images, rejected the highest and lowest estimates and averaged the remaining two to limit the effects of microlensing. For

two-image lenses they averaged the two estimates. Table 3 shows the estimated unmagnified H-band magnitude of each quasar. A12 did not apply a correction for variability. The typical variability of quasars can be obtained from measurements of their structure functions. Using the power-law fit of Vanden Berk et al. (2004) to the i-band structure function of SDSS quasars, a typical quasar sees a change of ~ 0.2 mag for a rest-frame time-lag of 1500 days. A change of 0.2 mag results in a change to the BH mass estimate of 0.04 dex, well below their typical error bar of 0.3 dex. $H-$band variability is still smaller, as the average amplitude decreases with increasing wavelength (see, e.g., Vanden Berk et al. 2004; MacLeod et al. 2010).

For our sub-sample of 3 targets, A12 obtained an absolute flux calibration of the near-IR spectra and measured the 5100Å continuum luminosity directly. For HS0810+2554 they fit a power-law to the continuum of the MDM CCDS spectrum (see §3.2) and extrapolated it to rest-frame 5100Å. For SBS0909+532 they calibrated the spectrum using the *HST* NICMOS H-band photometry, as the object never showed significant variations.

To obtain the rest-frame continuum UV luminosities at 1350Å and 1450Å, A12 flux-calibrated spectra and measured the flux by fitting straight lines to the rest-frame regions 1349 Å−1355Å(1440 Å−1460Å) for 1350Å (1450Å). A12 corrected these luminosities for foreground Galactic extinction from the dust maps of Schlegel et al. (1998). Errors in the continuum luminosity are dominated by the uncertainties in the magnification models, which are not well quantified. A12 assume a conservative error of 20% in each continuum luminosity estimate.

GPL10 obtained continuum luminosities at 5100Å for their objects with a similar approach. They fitted a power-law to the unmagnified *HST* photometry from CASTLES, using the lensing models of Peng et al. (2006). Compared to GPL10, the A12 luminosity estimates are 0.20 ± 0.05 dex smaller. The offset is likely caused by a combination of the differences in the lens models, in the prescription used to treat flux ratio anomalies, and in the use of the AGN SED template of Assef et al. (2010) instead of the power-law fits of Peng et al. (2006). This offset translates to 0.1 dex in BH mass, well below the uncertainties in SE mass measurements.

4.4. BH MASSES

The width of a broad emission line in a Type 1 AGN is the result of gravitational attraction by the supermassive BH on gas in the BLR. The mass $M_{\rm BH}$ of the BH from a virial assumption is

$$M_{\rm BH} \;=\; f\;\frac{R_{\rm BLR}(\Delta v)^2}{G}, \tag{2}$$

Δv is the velocity dispersion of the BLR gas from the width of the broad emission line and $R_{\rm BLR}$ is the distance from the BH to the BLR. The factor f is a scale of order unity that depends on the structure, kinematics and inclination of the BLR (see, e.g., Collin et al. 2006). The term $R_{\rm BLR}(\Delta v)^2/G$ is the virial product (VP) encapsulating all the observable quantities for a single object. The radius of the BLR can only be measured through RM (see, e.g., Peterson et al. 2004), but it correlates well with the continuum luminosity (see, e.g., Kaspi et al. 2005; Bentz et al. 2006, 2009; Zu et al. 2010).

For the broad Balmer lines A12 estimate the BLR radius from the relation $R_{\rm BLR}$ vs. $\lambda L_\lambda(5100\text{Å})$ (Bentz et al. (2009)), calibrated with a large sample of RM AGNs. In Eq. (2), f depends on either the FWHM or the line dispersion σ_l of the line, and on which line is used. To estimate $M_{\rm BH}$ from the width of Hβ, A12 use the f calibrations of Collin et al. (2006) for the FWHM and for σ_l. Although for σ_l a unique f of 3.85 for all AGNs suffices, Collin et al. (2006) argued that f is strongly dependent on the line profile shape for FWHM-based estimates.

A12 used the best-fit $f = 1.17$ for FWHM instead of the line-shape dependent calibrations because Denney et al. (2009) show that σ_l is affected by blending with other emission lines. For Hα there is no equivalent calibration of f. Therefore, A12 used the relation from Greene & Ho (2005) between the FWHMs of Hα and Hβ,

$$\mathrm{FWHM_{H\beta}} \;=\; (1.07 \pm 0.07) \times 10^3 \left(\frac{\mathrm{FWHM_{H\alpha}}}{10^3\ \mathrm{km\ s^{-1}}}\right)^{(1.03\pm0.03)} \mathrm{km\ s^{-1}} \tag{3}$$

to estimate the Hβ FWHM and then estimate $M_{\mathrm{BH}}(\mathrm{H}\alpha)$ using the same f and $R_{\mathrm{BLR}} - \mathrm{L}$ relation as for $M_{\mathrm{BH}}(\mathrm{H}\beta)$. Combining equations (2) and (3) with the $R_{\mathrm{BLR}} - \lambda L_\lambda(5100\text{Å})$ relation of Bentz et al. (2009),

$$M_{\mathrm{BH}}(\mathrm{H}\beta) \;=\; 6.71 \times 10^6\ f \left(\frac{\Delta v_{\mathrm{H}\beta}}{10^3\ \mathrm{km\ s^{-1}}}\right)^2 \left(\frac{\lambda L_\lambda(5100\text{Å})}{10^{44}\ \mathrm{erg\ s^{-1}}}\right)^{0.52} M_\odot \tag{4}$$

$$M_{\mathrm{BH}}(\mathrm{H}\alpha) \;=\; 7.68 \times 10^6\ f \left(\frac{\mathrm{FWHM_{H\alpha}}}{10^3\ \mathrm{km\ s^{-1}}}\right)^{2.06} \left(\frac{\lambda L_\lambda(5100\text{Å})}{10^{44}\ \mathrm{erg\ s^{-1}}}\right)^{0.52} M_\odot, \tag{5}$$

where in Eq. (4) $\Delta v_{\mathrm{H}\beta}$ can be either σ_l or the FWHM. Because Eq. (5) depends on the scaling relations for Hβ, f is the same as for FWHM$_{\mathrm{H}}\beta$ in Eq. (4). Table 3 shows the BH mass estimates based on Hα and Hβ for all objects in the sample.

For the UV/optical spectra A12 used the empirical $M_{\rm BH}$ calibrations of VP06 for the C IV broad emission line,

$$M_{\rm BH}({\rm C\,IV}) \;=\; 10^{\kappa}\;\left(\frac{\Delta v_{\rm C\,IV}}{10^3\ {\rm km\ s^{-1}}}\right)^2\;\left(\frac{\lambda L_\lambda(1350{\rm \AA})}{10^{44}\ {\rm erg\ s^{-1}}}\right)^{0.53}\;M_\odot, \tag{6}$$

where Δv is either FWHM or σ_l, and $\kappa = 6.66 \pm 0.01$ or 6.73 ± 0.01, respectively, for these line widths. κ implicitly contains f, which is assumed to be a constant. Whenever possible, A12 use the observed 1350Å flux to determine the continuum luminosity. Unfortunately 1350Å is not within the observed wavelength range of all the available spectra. For these, they estimated the continuum luminosity at 1350Å from the flux at 1450Å, as VP06. The C IV BH mass estimates are in Table 3 for both prescriptions used to measure the widths of C IV. Masses determined from the FWHM are highly consistent for both prescriptions, with a mean difference of 0.04 dex and a scatter of 0.02 dex; the average **B** mass estimates are smaller. The agreement is worse for σ_l, with a mean difference of 0.23 dex, in the sense that **B** is smaller, and the scatter 0.18 dex.

A12 estimate the uncertainties in BH mass estimates by propagating the errors in the velocity widths and in the continuum luminosities. For masses based on the width of the broad Balmer lines, they also propagate the uncertainties in the f-factor and in $R_{\rm BLR}$. Collin et al. (2006) determined that the uncertainty in f when using σ_l is 30%, while that in FWHM is 43%. For $R_{\rm BLR}$ they assume the intrinsic scatter of 0.11 dex estimated by Peterson (2010) for the radius-luminosity relation. Adding the uncertainties in f and $R_{\rm BLR}$ is not possible for the C IV estimates of the BH masses. Instead, add the measurement errors and the intrinsic scatter between C IV and RM BH mass estimates in quadrature.

Table 3. Hβ, Hα and CIV BH Mass Estimates

Object	$\log M_{\rm BH}/M_\odot$						
	FWHM$_{\rm C\,IV}$–p.A	FWHM$_{\rm C\,IV}$–p.B	$\sigma_{l,{\rm C\,IV}}$–p.A	$\sigma_{l,{\rm C\,IV}}$–p.B	FWHM$_{\rm H\beta}$	$\sigma_{l,{\rm H\beta}}$	FWHM$_{\rm H\alpha}$
Q0142–100	9.59 ± 0.32	9.51 ± 0.33	9.36 ± 0.29	9.36 ± 0.29	8.94 ± 0.30*	···	9.33 ± 0.23*
SDSS0246–0825	8.24 ± 0.33	8.23 ± 0.33	7.99 ± 0.29	7.81 ± 0.29	8.00 ± 0.31	···	8.08 ± 0.23
HS0810+2554	8.03 ± 0.32	7.99 ± 0.33	8.02 ± 0.29	7.87 ± 0.29	8.62 ± 0.22	8.54 ± 0.17	8.65 ± 0.22
SBS0909+532	8.51 ± 0.32	8.51 ± 0.32	8.76 ± 0.29	8.73 ± 0.29	9.29 ± 0.23	9.29 ± 0.17	9.15 ± 0.24
Q0957+561	9.02 ± 0.33	8.97 ± 0.32	8.98 ± 0.29	8.67 ± 0.29	8.86 ± 0.33	···	8.87 ± 0.23
HE1104–1805	9.37 ± 0.33	9.32 ± 0.32	9.04 ± 0.29	8.79 ± 0.29	8.77 ± 0.30	···	9.05 ± 0.23*
PG1115+080	8.83 ± 0.32	8.78 ± 0.32	8.64 ± 0.29	8.57 ± 0.29	8.66 ± 0.23	···	8.68 ± 0.22
SDSS1138+0314	7.71 ± 0.33‡	7.69 ± 0.33‡	8.15 ± 0.29‡	7.93 ± 0.29‡	8.50 ± 0.23	8.47 ± 0.19	8.22 ± 0.22
H1413+117	8.41 ± 0.45‡	8.39 ± 0.35‡	8.80 ± 0.29‡	8.17 ± 0.29‡	9.39 ± 0.33	···	9.29 ± 0.26
B1422+231	9.69 ± 0.32	9.65 ± 0.32	9.37 ± 0.29	9.27 ± 0.29	9.72 ± 0.38*	···	···
FBQ1633+3134	8.88 ± 0.32‡	8.82 ± 0.32‡	8.77 ± 0.29‡	8.29 ± 0.29‡	9.11 ± 0.28*	···	9.11 ± 0.27
Q2237+030	8.67 ± 0.33	8.63 ± 0.32	8.63 ± 0.29	8.34 ± 0.29	9.08 ± 0.39	···	9.38 ± 0.25*

Note. — All BH masses correspond to those obtained from Eq. (4), (5) and (6). No corrections were applied.

*Based on Group II line-width.

Using the sample of VP06, A12 find scatters of 0.32 dex and 0.28 dex for FWHM and σ_l respectively. VP06 found that the total scatter, including measurement errors, was 0.32 dex for both line-width characterizations of C IV, showing that the intrinsic scatter dominates over measurement errors, especially for FWHM estimates.

5. C IV BIASES IN BH MASS ESTIMATES

5.1. FWHM VS. σ_l MASSES

Given measurements for both FWHM and σ_l for C IV in all the A12 objects, the simplest test is to determine if there are any biases between them as BH mass estimators. Fig. 6 compares the C IV-based BH masses determined for both line-width estimates and for the two continuum and line blending prescriptions A and B, respectively.

There is a clear bias between prescriptions, such that most objects have a lower estimated BH mass if σ_l is used instead of the FWHM. The bias for **A** (**B**) width measurements is a constant offset $K = 0.13 \pm 0.06$ dex (0.24 ± 0.07 dex) or, equivalently, a factor of 1.3 (1.7).

The best-fit scatter is similar for both prescriptions, $S = 0.16$ dex for **A** and $S = 0.19$ dex for **B**. Because the logarithmic mass difference only depends on the line-widths and not on the continuum luminosities, the constant BH mass offsets K can also be expressed as an offset between the line-width descriptions. These values imply an offset of 0.10 ± 0.03 dex (0.16 ± 0.04 dex) between the FWHM and σ_l line-width characterizations of C IV for **A** (**B**).

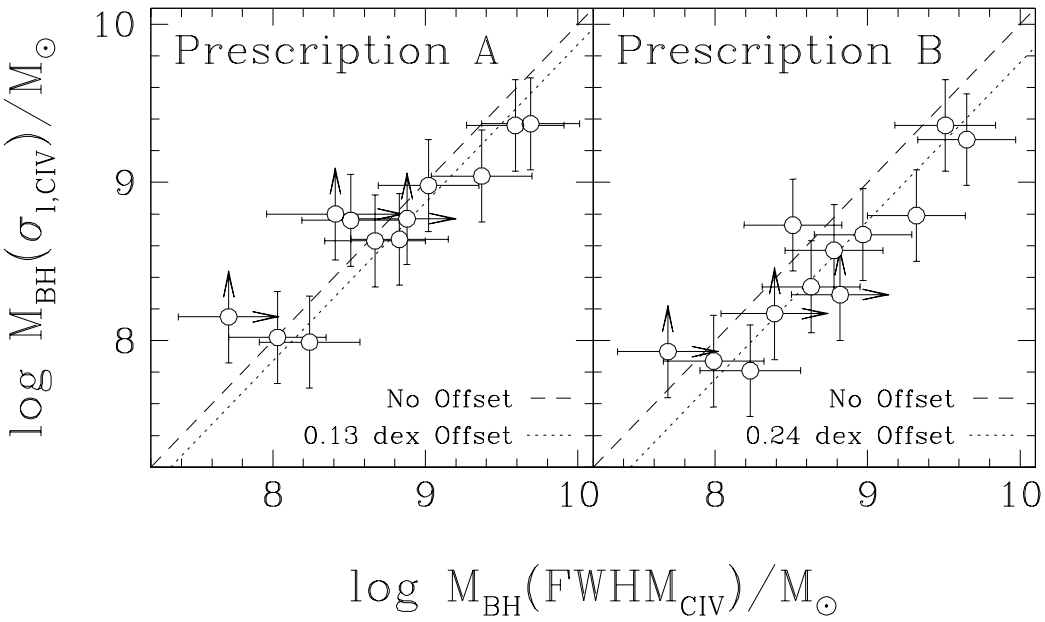

Fig. 6.— Comparison of C IV BH masses from the FWHM and σ_l for all objects in the sample, using the relations of VP06. The left (right) panel compares the BH mass estimates from **A** (**B**) line-width measurements of C IV. Masses are equal along the dashed line and the dotted line corresponds to the best fit offset. The objects with arrows have C IV line-width measurements that are lower bounds.

It is unsurprising that **A** yields a smaller offset between BH masses obtained from the FWHM and σ_l of C IV, as this prescription is modeled after that of VP06, who used their measurements to determine equation (6). However, given the similarity, the presence of a non-zero offset for **A** is puzzling. In the sample of VP06, the scatter is larger, 0.2 dex, and there is no offset (-0.02 ± 0.03 dex).

The large overlap in the mass and continuum luminosity ranges of the sample and that of VP06 suggest that there are no additional parameters. A12 found no correlation of the measured bias with BH mass, continuum luminosity or Eddington ratio. Also, no correlation with redshift, suggesting it is not an evolutionary trend. The only other major difference between the samples is the lensing by foreground galaxies. This should not be a problem, as quasars are quite compact and strong lensing magnifies the whole object. Microlensing by stars in the foreground galaxy could distort the shape of the C IV broad emission lines due to the spatial dependence of their velocity structure, but this is very unlikely for two reasons. First, the width of C IV is well below 10,000 km/s, constraining the location of the gas to a distance greater than $\gtrsim 10^3$ Schwarzschild radii (R_S) from the BH, whereas microlensing only has significant effects on scales below 100 R_S (Morgan et al. 2010). Second, the gas moving at the highest velocities is expected to be closest to the BH, so microlensing could magnify the wings of the line more than the core, and hence produce the inverse of what is seen by making σ_l too large compared to the FWHM.

5.2. C IV VS. Hα AND Hβ

Fig. 9 and 7 compare the mass estimates based on Hα and Hβ to those based on the width of C IV. Consider only UV BH masses based on prescription **B** width measurements of C IV. The FWHM based BH masses are almost

equal for prescriptions **A** and **B** (see §4.4), but they show a systematic offset for the σ_l estimates (see §5.1). Adopt **B** masses now, but the conclusions are unaltered under prescription **A** measurements. A12 assumed that the C IV FWHM mass estimates are unbiased, so those obtained from the **B** σ_l measurement of C IV have been shifted by the systematic offset of 0.24 dex derived earlier.

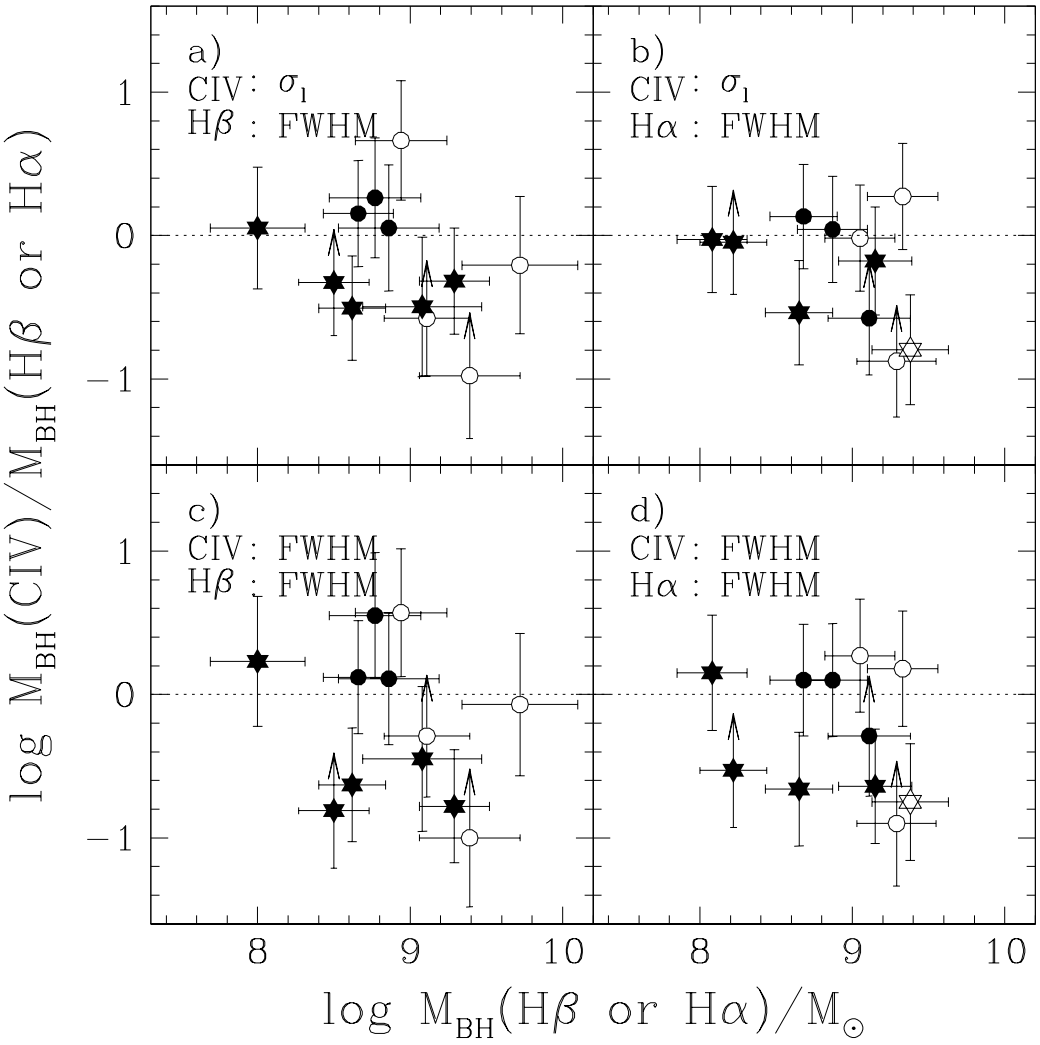

Fig. 7.— Ratio between the C IV and Hβ/Hα mass estimates as a function of the corresponding Balmer line mass estimate (Fig. 9).

A12 found no significant offset between the C IV-based and Hα- or Hβ-based masses when using only objects in Group I. The results are -0.12 ± 0.15, -0.11 ± 0.16, -0.15 ± 0.16 and -0.19 ± 0.18 dex for panels a), b), c) and d), respectively, of Fig. 7, with residual scatter of 0.30, 0.23, 0.46 and 0.38 dex. Including the objects in Group II does not change this conclusion, with best fit offsets of -0.05 ± 0.14, -0.13 ± 0.13, -0.07 ± 0.15 and -0.15 ± 0.14 dex, respectively, and residual scatters of 0.36, 0.33, 0.46 and 0.41 dex. The lack of offsets confirms that C IV FWHM BH masses are unbiased and that only those based on σ_l need to be corrected.

Are the residuals between the C IV and Balmer line masses correlated with any other observables? As an example, Fig. 8 shows the residuals as a function of the 1350Å and 5100Å continuum luminosities. Similar results obtain for redshift, Eddington ratio, blueshift of the C IV line, asymmetry of C IV (parametrized by the ratio of the widths red and blue of the centroid), and the ratio of the UV and optical continuum luminosities. Fig. 10 compares the C IV and Balmer line derived BH masses after rescaling the C IV masses using the best fit correlation. The corrections were of the form

$$\log M_{\rm BH}^{\rm Corr}({\rm C\,IV}) \;=\; \log M_{\rm BH}^{\rm VP06}({\rm C\,IV}) \;-\; b \;-\; a \log \frac{\lambda L_\lambda(1350\ {\rm \AA})}{\lambda L_\lambda(5100\ {\rm \AA})}. \qquad (7)$$

The agreement between the rest-frame UV and optical BH mass estimates after applying this correction is remarkable. The scatter of objects with Group I and non-lower bound line-widths decreased from 0.30 to 0.11, 0.23 to 0.10, 0.46 to 0.25 and 0.38 to 0.22 dex for panels a–d of Fig. 9 and 10, respectively. A12 find that the lowest scatter is between the BH masses estimated from the σ_l of C IV σ_l and the FWHM of either Balmer line. This supports the previous conclusion that σ_l C IV BH masses have small random errors, even if their systematic errors may be much larger than those of the FWHM estimates due to blending of emission lines. Such a small scatter places strong constraints on the strength of a possible correlation between the mass residuals and any tertiary parameter. Again, a slope other than unity is not required to describe the relation between the logarithm of the C IV and Balmer line BH masses.

There are 3 potential causes for a correlation of the mass ratio with the ratio of the continuum luminosities: i) extinction, ii) host contamination and iii) non-universal AGN SEDs. Extinction reduces the rest-frame UV continuum luminosity but has little effect on the rest-frame optical luminosity. Host contamination raises the optical luminosity but leaves the UV unchanged, as galaxies are typically brighter in the optical than in the UV. As to case iii), the radius of the BLR is determined by the flux of the ionizing continuum ($\lambda < 912$Å). The $R_{\rm BLR} - L$ relations used in equations (4), (5) and (6) implicitly assume a universal SED for all quasars, as they imply that the ionizing continuum can be predicted from the continuum luminosity at longer λ. This approximation is likely to be better for the rest-frame UV continuum than for the optical. All 3 cases would produce a slope of $a \simeq 0.5$ in eq. (7), simply representing the luminosity power indices in equations (4), (5) and (6). This is shallower than the observed slope but within 2σ of the best-fit relations. A larger sample is needed to fully determine if the slope of this correlation is statistically different from $\alpha \simeq 0.5$.

The sample is likely representative of observations of the general quasar population in terms of reddening and host contamination. Reddening by the lens galaxy will typically vary between quasar images. Falco et al. (1999) studied most of the objects in the sample and found that only two of them showed significant differential reddening: SBS0909+523 ($\Delta E(B-V) = 0.2$ mag for image B with respect to A) is an example. HS0810+2554 and SDSS1138+0314 were not part of the sample in Falco et al. (1999). A12 studied the latter object and concluded images B and C did not show evidence for differential reddening between them, but there is no information for the other objects. Lensing can also result in host contamination. The exact amount of host contamination depends on the size of the PSF and aperture used, the morphology of the lens and the surface brightness profile of the quasar host galaxy (see, e.g., Kochanek et al. 2001; Ross et al. 2009), however the zero-order effect is to not alter the amount of host contamination compared to an unlensed quasar.

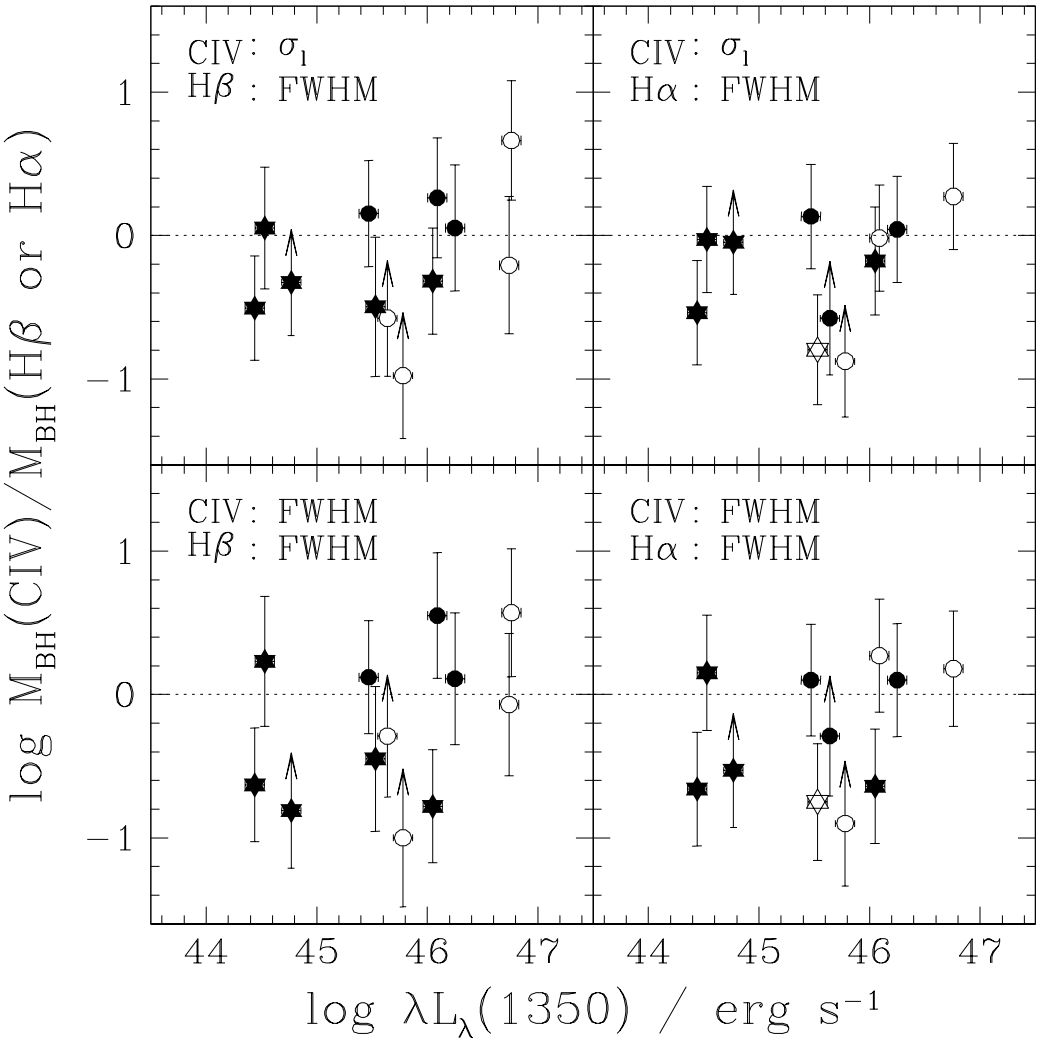

Fig. 8.— Same as Fig. 7, but as a function of the UV continuum luminosity.

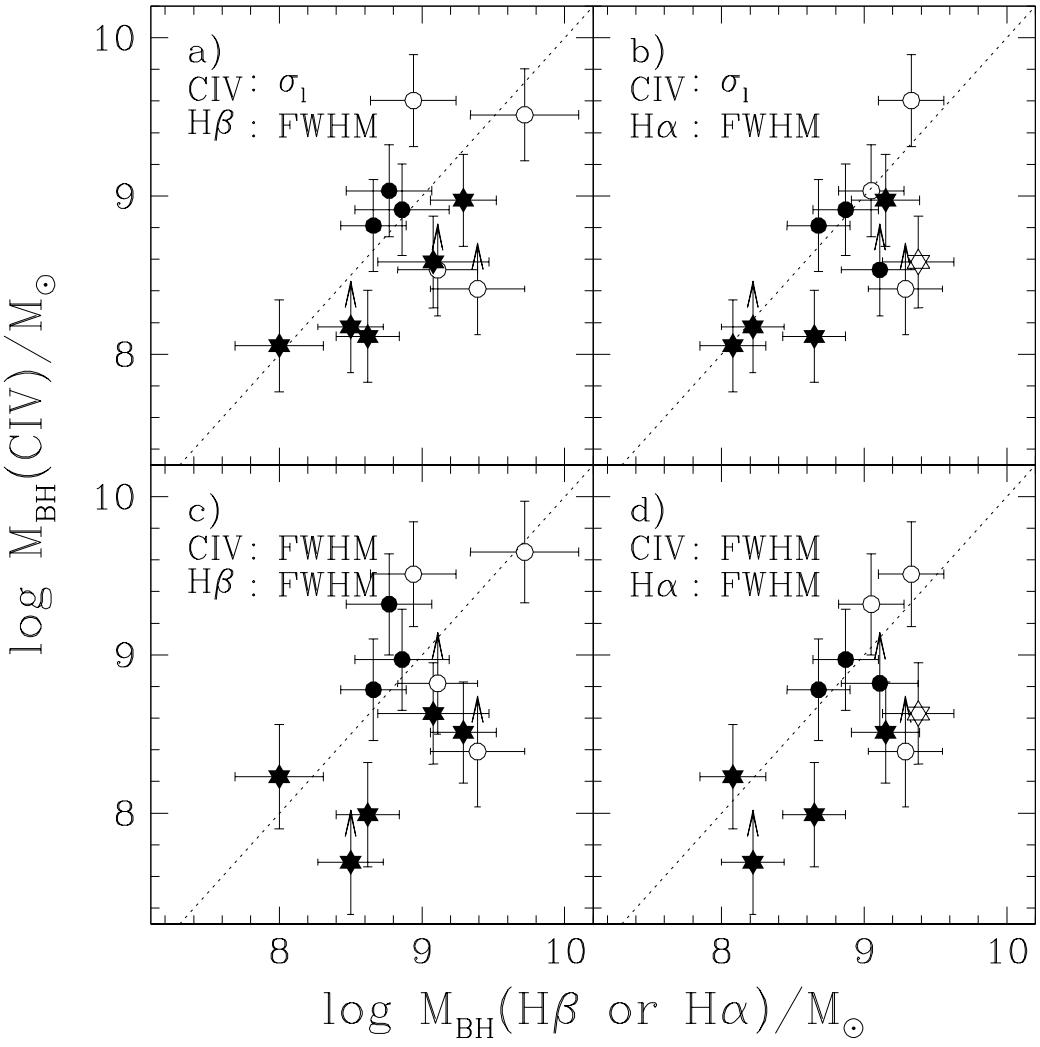

Fig. 9.— Comparison of BH masses estimated from **B** σ_l and FWHM of C IV and from the FWHM of Hα and Hβ. For the estimates based on σ_l for C IV the systematic offset of 0.24 dex in §5.1 was added. Solid symbols correspond to Group I and open symbols to Group II. Six-pointed stars mark objects not considered in GPL10. The dotted line shows where the BH masses are equal.

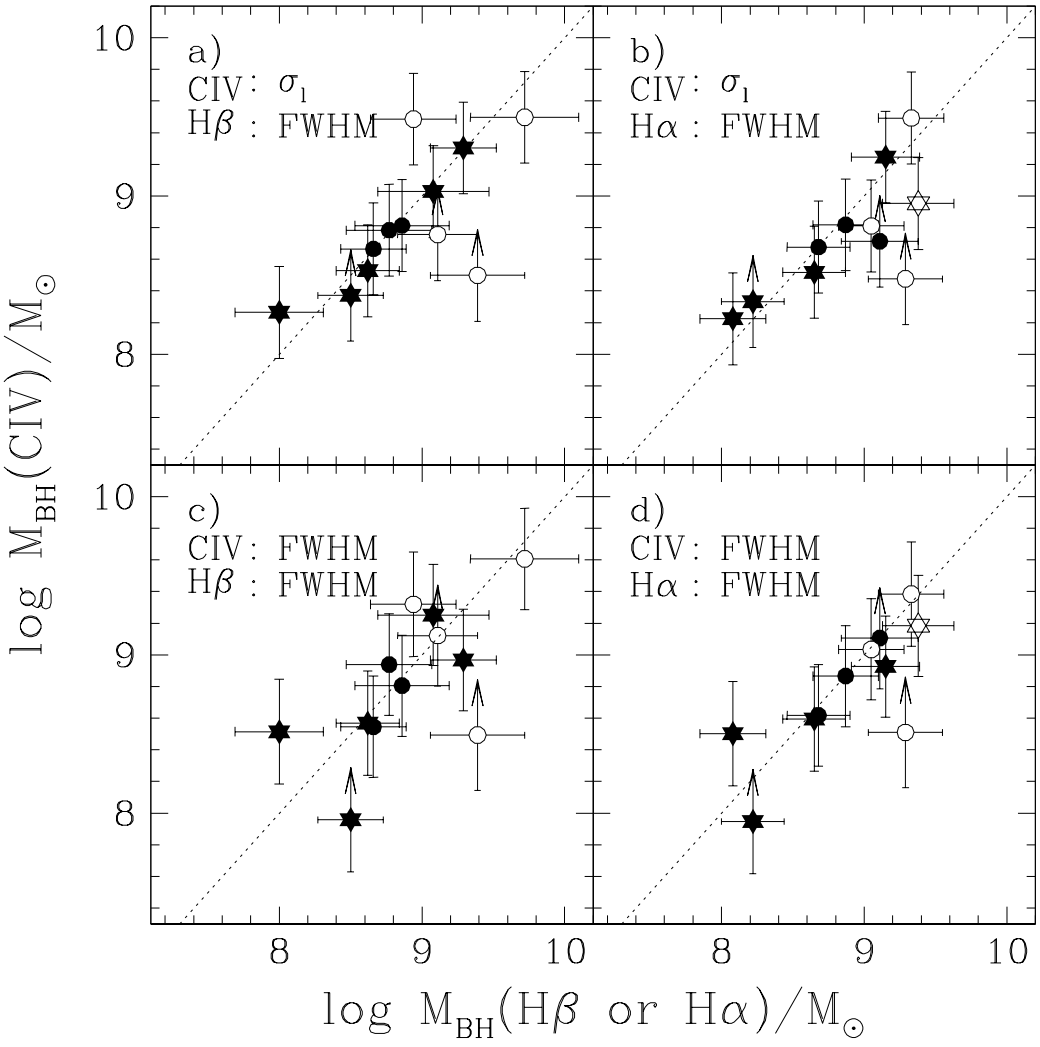

Fig. 10.— Same as Fig. 9, but after correcting the C IV BH masses for the dependence on the ratio of the UV to optical continuum luminosities.

6. OTHER STUDIES

VP06, and Dietrich & Hamann (2004) found that C IV derived BH masses are consistent with those obtained from the width of Hβ, and hence are a useful mass estimator. Shemmer et al. (2004), Netzer et al. (2007), Sulentic et al. (2007) and Dietrich et al. (2009), reached opposite conclusions. Shemmer et al. (2004) concluded that BH masses derived from C IV were poorly matched to those from Hβ and could be systematically different. They found that for a sample of narrow-line Seyfert 1 galaxies, C IV-based BH masses are larger by an average factor of ~ 3 compared to those obtained from Hβ. Dietrich et al. (2009) also found a large disagreement between the two estimates of the BH mass; the significance of this result is limited by the small number of objects (9) in their sample. Netzer et al. (2007), on the other hand, found no significant offset between the mass estimates, and argued there was also no discernible correlation between them. It is likely that many of the differences between the results of these studies are due to the use of different $R_{\rm BLR} - L$ calibrations, different f-factors, different prescriptions for measuring line widths, limited mass ranges and data quality.

A12 estimated BH masses using equations (4), (5) and (6). The left panel of Fig. 11 compares the C IV and Hβ BH masses derived for all these objects along with those in their sample. A clear correlation is observed for the complete ensemble of objects, albeit with a considerable scatter of 0.41 dex. The scatter is comparable with the 0.46 dex for the sample of C IV and Hβ FWHM-based BH masses. A linear fit to the left panel of Fig. 11 of the form

$$\log \frac{M_{\rm BH}({\rm C\,IV})}{10^8\ M_\odot} \ = \ m\ \log \frac{M_{\rm BH}({\rm H}\beta)}{10^8\ M_\odot} \ + \ n \tag{8}$$

yields a best-fit slope of $m = 0.89 \pm 0.08$ and intercept of $n = -0.09 \pm 0.08$.

Fig. 11 compares the C IV and Hβ derived masses after correcting for this correlation by applying equation (7). Although the strength of the correlation has not increased substantially ($r_s = 0.80$, $P_{\rm ran} = 6.4 \times 10^{-13}$), the scatter has decreased from 0.41 dex to 0.34 dex. This change is much more modest than that for the sample of lensed quasars, but this is likely due to the inhomogeneous prescriptions used to measure the width of the emission lines. A linear fit of the form of equation (8) to the relation between the BH mass estimates after applying the correction returns very similar parameters as before, with a best-fit slope of $m = 0.88 \pm 0.07$ and intercept of $n = 0.06 \pm 0.07$. Note that the measurement errors have again been scaled to make $\chi^2_\nu = 1$ before estimating the uncertainties in the fit parameters.

The inhomogeneity of the measurements can be a very significant source of scatter in the comparisons. With homogeneously analyzed, high SNR spectra, the difference between the line widths is not the dominant source of scatter in the comparison between C IV and Balmer line-based BH mass estimates. It is useful to assess whether the C IV and Hβ line widths are correlated in this combined sample.

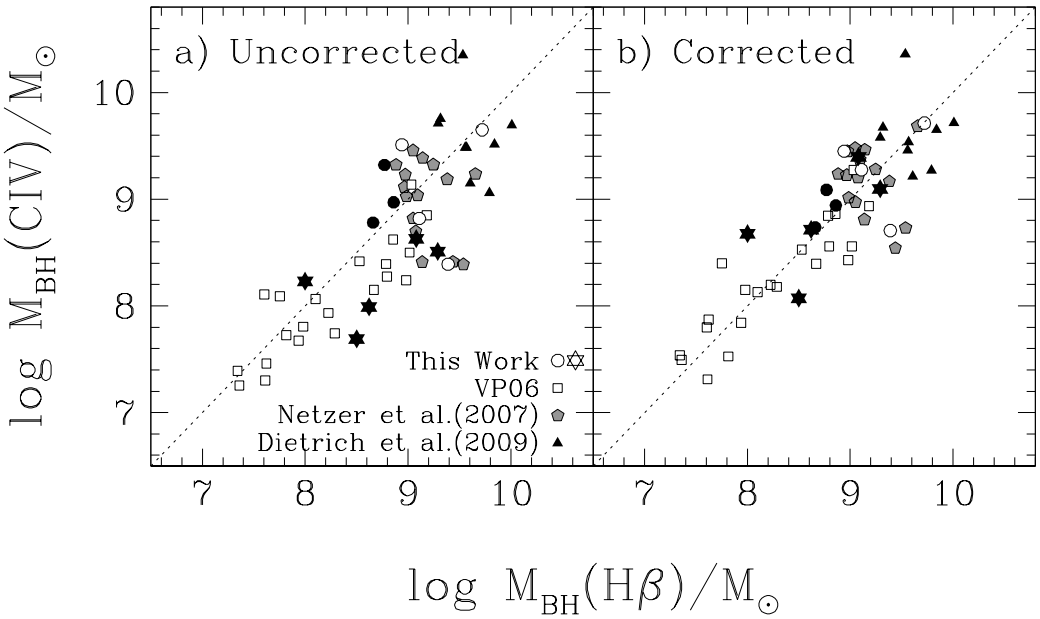

Fig. 11.— Panel *a*) shows the BH masses estimated using Eq. (4), (5) and (6) for the objects in VP06 (*open squares*), Netzer et al. (2007) (*solid gray pentagons*) and Dietrich et al. (2009) (*solid black triangles*) for which this was possible. Objects in A12 are solid and open six-pointed stars and circles. The dotted line shows where the masses are equal. Panel *b*) shows the results after applying continuum slope corrections.

7. NEXT STUDIES

The A12 results were the inspiration to pursue measurements similar to those acquired with LUCIFER, at Magellan. We started collecting high-SNR HK longslit spectroscopy with Magellan/MMIRS of a sample of quasar lenses. The initial target list contains 7 quasar lenses (Table 4) extracted from CASTLES.

The MMT and Magellan Infrared Spectrograph (MMIRS) is a wide-field near-IR imager and multi-object spectrograph with a maximum resolution of R$\sim$ 3000 with a $0\farcs4$ slit.

In two runs in 2011 and one in early 2012, we obtained useful spectra for all the targets in our list. We oriented the slit to include 2 images in each system. The typical seeing during the observations was $\sim 0\farcs6$.

Fig. 12 shows 2 examples of reduced MMIRS spectra. The analysis to extract BH mass estimates is in progress.

Table 4. MMIRS Target list

Object	RA	DEC	H (mag)	max. sep. (″)	z_{im}
HE0512-3329	05:14:10.8	-33:26:23	16.3	0.7	1.57
LBQS1009-0252	10:12:15.7	-03:07:02	17.8	1.54	2.74
Q1017-207	10:17:24.1	-20:47:00	16.8	0.9	2.55
HE1104-1805	11:06:33.5	-18:21:24	16.2	3.2	2.32
SDSS1138+0314	11:38:03.7	+03:14:58	18.4	1.34	2.44
PMNJ1632-0033	16:32:57.7	-00:33:21.1	19.	1.5	3.42
PMNJ1838-3427	18:38:28.5	-34:27:41.6	17.	1.0	2.78

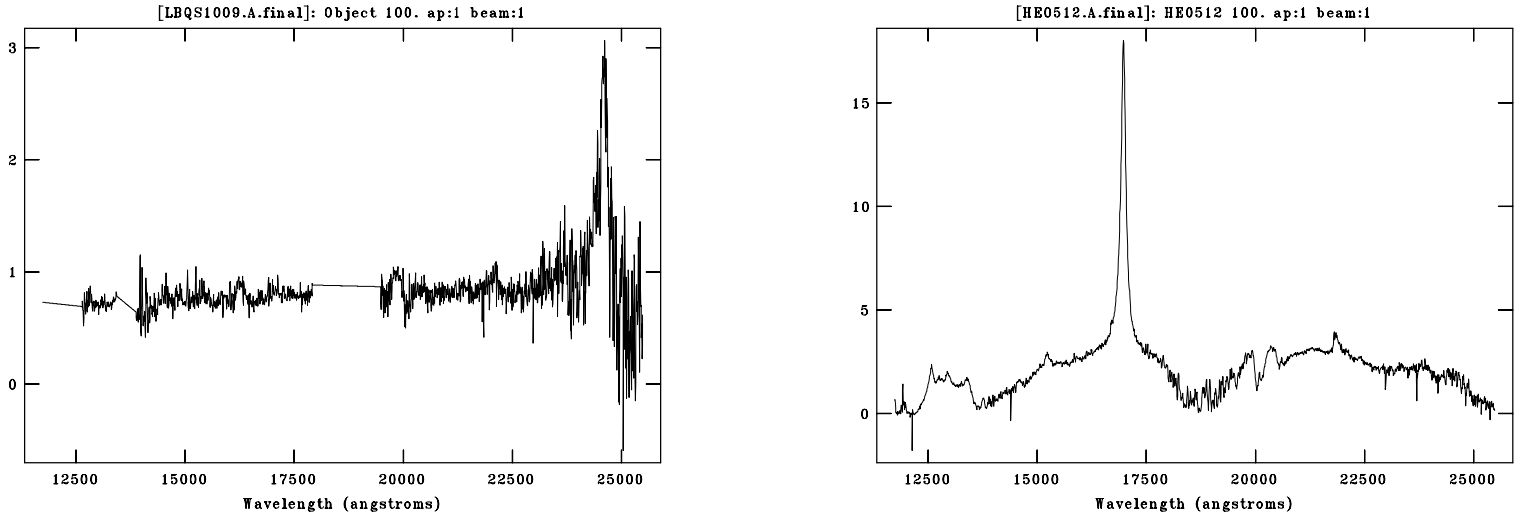

Fig. 12.— Left: MMIRS HK spectrum for the double LBQS1009-0252, image A, with Hα at 2.47 μm, redshifted by the quasar redshift, $z = 2.74$. Right: MMIRS HK spectrum for the double HE0512-3329, image A, with Hα at 1.70 μm, redshifted by the quasar redshift, $z = 1.57$.

REFERENCES

Abazajian, K. N., et al. 2009, ApJS, 182, 543

Allington-Smith, J., et al. 1994, PASP, 106, 983

Ageorges, N., Seifert, W., Juette, M., Knierim, V., Lehmitz, M., Germeroth, A., Buschkamp, P., Polsterer, K., Pasquali, A., Naranjo, V., Gemperlein, H., Hill, J., Feiz, C., Hofmann, R., Laun, W., Lederer, R., Lenzen, R.d, Mall, U., Mandel, H. , Mueller, P., Quirrenbach, A., Schaeffner, L., Storz, C. ,Weiser, P. : LUCIFER1 commissioning at the LBT, 2010, Proc. SPIE, 7735-56, to be published

Assef, R. J., et al. 2010, ApJ, 713, 970

Bentz, M. C., et al. 2009, ApJ, 705, 199

Bentz, M. C., Peterson, B. M., Pogge, R. W., Vestergaard, M., & Onken, C. A. 2006, ApJ, 644, 133

Blandford, R. D., & McKee, C. F. 1982, ApJ, 255, 419

Boroson, T. A., & Green, R. F. 1992, ApJS, 80, 109

Botti, I., Lira, P., Netzer, H., & Kaspi, S. 2010, IAU Symposium, 267, 198

Cappellari, M., Verolme, E. K., van der Marel, R. P., Kleijn, G. A. V., Illingworth, G. D., Franx, M., Carollo, C. M., & de Zeeuw, P. T. 2002, ApJ, 578, 787

Collin, S., Kawaguchi, T., Peterson, B. M., & Vestergaard, M. 2006, A&A, 456, 75

Decarli, R., Labita, M., Treves, A., & Falomo, R. 2008, MNRAS, 387, 1237

Denney, K. D., Peterson, B. M., Dietrich, M., Vestergaard, M., & Bentz, M. C. 2009, ApJ, 692, 246

Dietrich, M., Mathur, S., Grupe, D., & Komossa, S. 2009, ApJ, 696, 1998

Dietrich, M., Crenshaw, D. M., & Kraemer, S. B. 2005, ApJ, 623, 700

Dietrich, M., & Hamann, F. 2004, ApJ, 611, 761

Dietrich, M., Appenzeller, I., Vestergaard, M., & Wagner, S. J. 2002, ApJ, 564, 581

Dressler, A., Hare, T., Bigelow, B. C., & Osip, D. J. 2006, Proc. SPIE, 6269,

Eigenbrod, A., Courbin, F., Meylan, G., Vuissoz, C., & Magain, P. 2006, A&A, 451, 759

Eigenbrod, A., Courbin, F., Sluse, D., Meylan, G., & Agol, E. 2008, A&A, 480, 647

Fadely, R., Keeton, C. R., Nakajima, R., & Bernstein, G. M. 2010, ApJ, 711, 246

Falco, E. E., et al. 2001, Gravitational Lensing: Recent Progress and Future Go, 237, 25

Falco, E. E., et al. 1999, ApJ, 523, 617

Ferrarese, L., & Merritt, D. 2000, ApJ, 539, L9

Fine, S., Croom, S. M., Bland-Hawthorn, J., Pimbblet, K. A., Ross, N. P., Schneider, D. P., & Shanks, T. 2010, MNRAS, accepted (arXiv:1005.5287)

Gallagher, S. C., Richards, G. T., Hall, P. B., Brandt, W. N., Schneider, D. P., & Vanden Berk, D. E. 2005, AJ, 129, 567

Gaskell, C. M. 1982, ApJ, 263, 79

Gebhardt, K., et al. 2000, ApJ, 539, L13

Goicoechea, L. J., Gil-Merino, R., & Ullán, A. 2005, MNRAS, 360, L60

Graham, A. W., Onken, C. A., Athanassoula, E., & Combes, F. 2011, MNRAS, 412, 2211

Graham, A. W. 2007, MNRAS, 379, 711

Granato, G. L., De Zotti, G., Silva, L., Bressan, A., & Danese, L. 2004, ApJ, 600, 580

Greene, J. E., Peng, C. Y., & Ludwig, R. R. 2010, ApJ, 709, 937 (GPL10)

Greene, J. E., & Ho, L. C. 2005, ApJ, 630, 122

Gültekin, K., et al. 2009, ApJ, 698, 198

Hopkins, P. F., Hernquist, L., Cox, T. J., Di Matteo, T., Martini, P., Robertson, B., & Springel, V. 2005, ApJ, 630, 705

Hopkins, P. F., Robertson, B., Krause, E., Hernquist, L., & Cox, T. J. 2006, ApJ, 652, 107

Hopkins, P. F., Hernquist, L., Cox, T. J., & Kereš, D. 2008, ApJS, 175, 356

Horne, K., Peterson, B.M., Collier, S., & Netzer, H. 2004, PASP 116, 465 - 476.

Jahnke, K., & Maccio, A. 2010, arXiv:1006.0482

Jarvis, M. J., & McLure, R. J. 2006, MNRAS, 369, 182

Jiang, G., & Kochanek, C. S. 2007, ApJ, 671, 1568

Kaspi, S., Brandt, W. N., Maoz, D., Netzer, H., Schneider, D. P., & Shemmer, O. 2007, ApJ, 659, 997

Kaspi, S., Maoz, D., Netzer, H., Peterson, B. M., Vestergaard, M., & Jannuzi, B. T. 2005, ApJ, 629, 61

Kaspi, S., Smith, P. S., Netzer, H., Maoz, D., Jannuzi, B. T., & Giveon, U. 2000, ApJ, 533, 631

Keeton, C. R. 2001, arXiv:astro-ph/0102340

Kelly, B. C., Bechtold, J., & Siemiginowska, A. 2009, ApJ, 698, 895

Kelson, D. D. 2003, PASP, 115, 688

Kochanek, C.S., Schneider, P., Wambsganss, J., 2004, Part 2 of Gravitational Lensing: Strong, Weak & Micro, Proceedings of the 33rd Saas-Fee Advanced Course, G. Meylan, P. Jetzer & P. North, eds. (Springer-Verlag: Berlin)

Kochanek, C. S., Keeton, C. R., & McLeod, B. A. 2001, ApJ, 547, 50

Koopmans, L. V. E., et al. 2009, ApJ, 703, L51

Laor, A., Bahcall, J. N., Jannuzi, B. T., Schneider, D. P., Green, R. F., & Hartig, G. F. 1994, ApJ, 420, 110

Lehár, J., et al. 2000, ApJ, 536, 584

Leighly, K. M., & Moore, J. R. 2004, ApJ, 611, 107

MacLeod, C. L., et al. 2010, arXiv:1004.0276

Maiolino, R. Gallerani, S., Neri, R. Cicone, C., Ferrara, A., Genzel, R., Lutz, D., Sturm, E., Tacconi, L. J., Walter, F., Feruglio, C., Fiore, F. & Piconcelli, E. 2012, MNRAS, 425, 66

Marconi, A., Axon, D. J., Maiolino, R., Nagao, T., Pastorini, G., Pietrini, P., Robinson, A., & Torricelli, G. 2008, ApJ, 678, 693

Marconi, A., & Hunt, L. K. 2003, ApJ, 589, L21

Martini, P., et al. 2011, PASP, 123, 187

Marziani, P., Sulentic, J. W., Dultzin-Hacyan, D., Calvani, M., & Moles, M. 1996, ApJS, 104, 37

McGill, K. L., Woo, J.-H., Treu, T., & Malkan, M. A. 2008, ApJ, 673, 703

Mediavilla, E. et al. 2010, in preparation.

Merritt, D., & Ferrarese, L. 2001, The Central Kiloparsec of Starbursts and AGN: The La Palma Connection, 249, 335

Mogren, K., et al. in preparation.

Morgan, C. W., Kochanek, C. S., Morgan, N. D., & Falco, E. E. 2010, ApJ, 712, 1129

Morgan, C. W., Byard, P. L., DePoy, D. L., Derwent, M., Kochanek, C. S., Marshall, J. L., O'Brien, T. P., & Pogge, R. W. 2005, AJ, 129, 2504

Netzer, H., Lira, P., Trakhtenbrot, B., Shemmer, O., & Cury, I. 2007, ApJ, 671, 1256

Oke, J. B., & Gunn, J. E. 1982, PASP, 94, 586

Onken, C. A., & Kollmeier, J. A. 2008, ApJ, 689, L13

Peng, C. Y. 2010, arXiv:1002.2664

Peng, C. Y. 2007, ApJ, 671, 1098

Peng, C. Y., Impey, C. D., Rix, H.-W., Kochanek, C. S., Keeton, C. R., Falco, E. E., Lehár, J., & McLeod, B. A. 2006, ApJ, 649, 616

Peterson, B. M. 2010, IAU Symposium, 267, 151

Peterson, B. M., et al. 2004, ApJ, 613, 682

Peterson, B. M. 1993, PASP, 105, 247

Richards, G. T., Vanden Berk, D. E., Reichard, T. A., Hall, P. B., Schneider, D. P., SubbaRao, M., Thakar, A. R., & York, D. G. 2002, AJ, 124, 1

Ross, N. R., Assef, R. J., Kochanek, C. S., Falco, E., & Poindexter, S. D. 2009, ApJ, 702, 472

Rusin, D., Kochanek, C. S., & Keeton, C. R. 2003, ApJ, 595, 29

Seifert, W., et al. 2003, Proc. SPIE, 4841, 962

Schlegel, D. J., Finkbeiner, D. P., & Davis, M. 1998, ApJ, 500, 525

Shankar, F., Weinberg, D. H., & Miralda-Escudé, J. 2009, ApJ, 690, 20

Shemmer, O., Netzer, H., Maiolino, R., Oliva, E., Croom, S., Corbett, E., & di Fabrizio, L. 2004, ApJ, 614, 547

Shen, Y., Greene, J. E., Strauss, M. A., Richards, G. T., & Schneider, D. P. 2008, ApJ, 680, 169

Somerville, R. S., Hopkins, P. F., Cox, T. J., Robertson, B. E., & Hernquist, L. 2008, MNRAS, 391, 481

Sulentic, J. W., Bachev, R., Marziani, P., Negrete, C. A., & Dultzin, D. 2007, ApJ, 666, 757

Tonry, J. L. 1998, AJ, 115, 1

Tremaine, S., et al. 2002, ApJ, 574, 740

Tytler, D., & Fan, X.-M. 1992, ApJS, 79, 1

Ulrich, M.-H., & Horne, K. 1996, MNRAS 283, 748 - 758

Vacca, W. D., Cushing, M. C., & Rayner, J. T. 2003, PASP, 115, 389

Vanden Berk, D. E., et al. 2004, ApJ, 601, 692

van der Marel, R. P., & Franx, M. 1993, ApJ, 407, 525

Vestergaard, M., & Peterson, B. M. 2006, ApJ, 641, 689 (VP06)

Vestergaard, M., Wilkes, B. J., & Barthel, P. D. 2000, ApJ, 538, L103

Weymann, R. J., Carswell, R. F., & Smith, M. G. 1981, ARA&A, 19, 41

Wilhite, B. C., Brunner, R. J., Grier, C. J., Schneider, D. P., & vanden Berk, D. E. 2008, MNRAS, 383, 1232

Wills, B. J., & Brotherton, M. S. 1995, ApJ, 448, L81

Wills, B. J., Netzer, H., Brotherton, M. S., Han, M., Wills, D., Baldwin, J. A., Ferland, G. J., & Browne, I. W. A. 1993, ApJ, 410, 534

Wills, B. J., & Browne, I. W. A. 1986, ApJ, 302, 56

Wills, B. J., Netzer, H., & Wills, D. 1985, ApJ, 288, 94

Wilkes, B. J. 1984, MNRAS, 207, 73

Wisotzki, L., Koehler, T., Ikonomou, M., & Reimers, D. 1995, A&A, 297, L59

Woo, J.-H., Treu, T., Malkan, M. A., Ferry, M. A., & Misch, T. 2007, ApJ, 661, 60

Yip, C. W., et al. 2004, AJ, 128, 2603

Zu, Y., Kochanek, C. S., & Peterson, B. M. 2010, arXiv:1008.0641